Xon Junites

I 8. 017

MINN A

Q2

240

Import factor 1.275

Physica B 472 (2015) 84-90 COH



Contents lists available at ScienceDirect

Physica B

めなん

journal homepage: www.elsevier.com/locate/physb



Effects of strain on the Schwinger pair creation in graphene



P. Fanbanrai a, A. Hutem a,c, S. Boonchui a,b,*

- ^a Department of Physics, Faculty of Science, Kasetsart University, Bangkok 10900, Thailand
- ^b Center of Excellence in Forum for Theoretical Science, Chulalongkorn University, Bangkok 10330, Thailand
- ^c Physics Division, Faculty of Science and Technology, Phetchabun Rajabhat University, Phetchabun 67000, Thailand

ARTICLEINFO

Article history: Received 5 December 2014 Received in revised form 7 May 2015 Accepted 18 May 2015 Available online 27 May 2015

Keywords: Strained graphene Schwinger pair creation

ABSTRACT

The effects of strain on mechanically deformed graphene are determined by looking at how the strain affects the amplitude of the Schwinger two particle pair state. The influences of the lattice distortions, such as isotropic tensile strain ϵ_{is} , shear strain ϵ_{ss} , uniaxial armchair strain ϵ_{as} , and zigzag strain ϵ_{zs} , on the photon emission spectrum have been analyzed. We find that the intensities of the emission increases or decreases when compared to those of the unstrained graphene, depending on the type of strain applied. Thus the structure of energy band, the frequencies of the photons and the emission spectrum can be controlled by use of the different strains.

© 2015 Elsevier B.V. All rights reserved.

1. Introduction

Graphene [1,2] is a new material having fascinating properties. It offers a challenge to both fundamental and applied sciences. Many of its properties can be engineered to create novel physical scenarios in condensed matter setting: its chiral and Dirac-like energy dispersion relations close to the Fermi energy leads to Klein tunneling [3], Veselago lensing [4] and pseudo-magnetic fields [5]. The last leads to prominent platforms for ultrafast photonics and opto-electronics [6–8], etc.

Other interesting properties occur when strains are applied. These occur when the crystal is compressed or stretched out of equilibrium. The resulting stiffness tensor provides for a constitutive relation between the applied stress and the final strain state. The strain can significantly affect the Fermi line, e.g., deformed from the isotropic circle towards an elliptical shape. The low-energy electronic properties are then described by a generalized two-dimensional Weyl Hamiltonian with two Fermi velocities, defined along the principal directions [9]. Another effect of the distortion of the crystal lattice is that the Dirac points are displaced from the corners of the unstrained Brillouin [10] and produce a gap in the energy dispersion when the order of strain is 20%.

Recently, the optoelectronic properties [10–12] of graphene have been studied using a formulation based on treating the BCS state as the result of the creation of an electron–positron pair. This corresponds to the use of quantum electrodynamics as formulated by Schwinger [13]. We use a generalized two dimensional Weyl

Hamiltonian to describe a mechanically deformed (by pressure) graphene sheet. The amplitude of the Schwinger pair can be modified by applying a strain to the graphene.

The paper is organized as follows: we begin with a theoretical discussion of the Weyl–Dirac Hamiltonian when the graphene is strained by a tensile isotropic strain, a shear strain, a uniaxial armchair strain or by a zigzag strain. In Section 2, we determine the intensity of photon emission on the graphene's plane for each angle in Schwinger's pair creations, obtaining the effect of deformed lattices. We show the results of the calculations in Section 3. Finally the results are discussed in Section 4.

2. Asymmetric Weyl-Dirac fermions in deformed graphene

Our formulation takes into account the effects of deforming the lattice. This will lead to a modification of the hopping. Modification of the hopping energies between different sites will in turn lead to new terms in the original Hamiltonian in the tight-binding formulation:

$$\mathbf{H} = -\sum_{\langle i,j\rangle} t \, (\overrightarrow{l\delta_{ij}}) \, (\hat{a}_i^{\dagger} \, \hat{b}_j \, + \, \hat{b}_j^{\dagger} \, \hat{a}_i^{\dagger}), \tag{1}$$

where $\vec{\delta}_{ij}$ is the *i*th nearest-neighbor vector of the *j*th atom, and $t(\vec{\delta}_{ij})$ is the strained hopping energy due to strain. The length and direction of the three nearest-neighbor vector $\vec{\delta}_{ij}$ transform under strain according to $\vec{\delta}_{ij} \simeq (1 + \epsilon) \cdot \vec{\delta}_{0}$ where $\vec{\delta}_{0}$ represents a nearest-neighbor vector in the non-deformed graphene plane, and ϵ is the strain tensor [14]. In Cartesian coordinate system, we assume the

^{*} Corresponding author.

E-mail address: fscistb@ku.ac.th (S. Boonchui).

x-axis is along graphene armchair direction and the *y*-axis is along graphene's zigzag (Fig. 1). In reciprocal space, the variation of hopping energy with inter carbon distance is $t(|\vec{\delta}_{ij}|) = t_0 \exp[-\beta(|\vec{\delta}_{ij}|/a-1)]$ with a=1.42 Å being the unstrained nearest-neighbor separation, $t_0=2.7$ eV, and $\beta\approx 3$ [15,16]. The hopping perturbation δt_i can be obtained by expanding $t(|\vec{\delta}_{ij}|)$ and keeping the first order:

$$t\left(a+\Delta\delta_{ij}\right)\simeq t_0\left(1-(\beta/a)(|(1+\epsilon)\cdot\overrightarrow{\delta_{i0}}|-|\overrightarrow{\delta_{i0}}|)\right), \tag{2}$$

with $\Delta \delta_{ij}$ being the variation of bond length. By introducing Fourier transform of the creation and annihilation operators

$$\hat{a}_{i} = \sum_{Q} \hat{a}_{Q} e^{i\vec{R}_{i}'\vec{Q}} / \sqrt{N}, \quad \hat{b}_{i} = \sum_{Q} \hat{b}_{Q} e^{i(\vec{R}_{i}' + \vec{\delta}_{i}')\cdot\vec{Q}} / \sqrt{N}, \quad (3)$$

the Hamiltonian Eq. (1) in the reciprocal space can be written as

$$\mathbf{H} = \sum_{\mathbf{Q}} (\hat{a}_{\mathbf{Q}}^{\dagger} \hat{b}_{\mathbf{Q}}^{\dagger}) \mathcal{H} \begin{pmatrix} \hat{a}_{\mathbf{Q}} \\ \hat{b}_{\mathbf{Q}} \end{pmatrix}, \tag{4}$$

where \overrightarrow{Q} is a wave vector in the first Brillouin zone and $\mathcal H$ is a tensor given by

$$\mathcal{H} \simeq -\sum_{j=1,2,3} \begin{pmatrix} 0 & t(a+\Delta\delta_i)e^{-i\vec{Q}\cdot\vec{\delta}'_j} \\ t(a+\Delta\delta_i)e^{i\vec{Q}\cdot\vec{\delta}'_j} & 0 \end{pmatrix}.$$
 (5)

By expanding $e^{-i\vec{Q}\cdot\vec{s}'_j}$ with respect to δ_j and keeping only the first order terms, we obtain the following single particle Hamiltonian near the \vec{K} points:

$$\mathcal{H} = \sum_{\mu=1,2} \hbar \vec{V}_{\mu} \cdot \vec{k} \, \sigma^{\mu} + \frac{e}{c} \vec{A}_{pse} \cdot \vec{\sigma} \,. \tag{6}$$

This is the Weyl–Dirac equation for the deformed graphene where σ^{μ} 's are the Pauli matrices, i.e.,

$$\sigma^{1} = \begin{pmatrix} 0 & 1 \\ 1 & 0 \end{pmatrix}, \quad \sigma^{2} = \begin{pmatrix} 0 & -i \\ i & 0 \end{pmatrix}, \tag{7}$$

and the 2D-velocities $\vec{v}_{\mu} = (v_{\mu}^{x}, v_{\mu}^{y})$ is defined by its components as

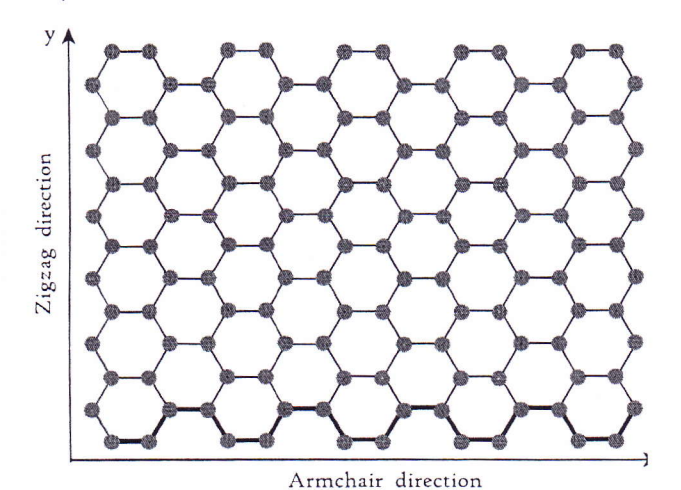


Fig. 1. Schematic of graphene armchair and zigzag directions.

$$v_1^x = -v_F \left(\frac{1}{2} \beta \epsilon_{xy} - \frac{2\pi}{3\sqrt{3}} \epsilon_{xy} \right),$$

$$v_1^y = v_F \left(1 - \frac{1}{4} \beta (\epsilon_{xx} + 3\epsilon_{yy}) - \frac{2\pi}{3\sqrt{3}} \epsilon_{yy} \right)$$
(8)

and

$$\begin{split} v_2^x &= v_F \left(1 - \frac{1}{4} \beta (3 \epsilon_{xx} + \epsilon_{yy}) + \frac{2\pi}{3\sqrt{3}} \epsilon_{yy} \right), \\ v_2^y &= -v_F \left(\frac{1}{2} \beta (\epsilon_{xy} - \frac{2\pi}{3\sqrt{3}} \epsilon_{xy} \right). \end{split} \tag{9}$$

As we have seen, the Weyl–Dirac Hamiltonian is described by the velocities $\vec{v_1}$ and $\vec{v_2}$ which are defined in terms of four elements of the strain tensors, ϵ_{xx} , ϵ_{xy} , ϵ_{yx} and ϵ_{yy} . Those velocities reduce to $\vec{v_1} = (0, v_F)$ and $\vec{v_2} = (v_F, 0)$ in the case of vanishing strain. Eq. (6), thus, becomes the Dirac Hamiltonian with the pseudo-vector potential \vec{A}_{pse} given by

$$\vec{A}_{pse} = \frac{cv_F \pi \hbar}{ea} \left(\left(\frac{4}{3\sqrt{3}} \epsilon_{yy} + \frac{\beta}{2\pi} (\epsilon_{xx} - \epsilon_{yy}) \right) \cdot \left(\frac{4}{3\sqrt{3}} \epsilon_{xy} + \frac{\beta}{\pi} \epsilon_{xy} \right) \right). \tag{10}$$

The reciprocal space is shifted from the traditional Dirac points. The nature of the contours of the strained band structure has been discussed in ref. [17]. For non-uniform strain, the Landau level structure is described as one modified by a non-uniform effective magnetic field [18]. For strongly deformed lattice [19], the effect of hopping mechanism for next-nearest neighbors leads anti-symmetric properties of the energy spectrum to around zero energy.

In this paper, a moderate deformation, $|\epsilon| < 0.2$, is assumed. This allows for linearization of the hopping energy around its non-deformed value t, and $\partial t/\partial a \simeq -5$ eV/Å. The essential point of our approach is that the uniform strain in the graphene lattice is capable of changing the velocities \vec{v}_{k} 's. In case of uniform strain, the pseudo-vector potential appeared in the Weyl-Dirac equation is uniform and then there is no pseudo-magnetic field present $(\vec{B}_{pse} = \vec{\nabla} \times \vec{A}_{pse})$. Thus the optical property can be controlled by the mechanical strains. Thus, this draws our attention to the deformation of Fermi line from the isotropic circle to an elliptical shape due to the applying strains (Fig. 2). Each item in the figure shows the effects of different types of strain on the shape of the Fermi line.

The general solution of the Weyl–Dirac equation, Eq. (6), yields the energy dispersion:

$$E_{\kappa}(\vec{k}) = \kappa \hbar \sqrt{(\vec{v}_1 \cdot \vec{k})^2 + (\vec{v}_2 \cdot \vec{k})^2}$$

$$\tag{11}$$

where $\kappa=\pm 1$ plays the role of the band index for positive or negative energy, i.e., conduction or valence. Analogous to the spinor, the two components eigenstates can be written as

$$|\chi_{\kappa}(\overrightarrow{k})\rangle = \frac{1}{\sqrt{2}} \left(e^{-i\Phi(\overrightarrow{k}_{\kappa})} \right) \tag{12}$$

where $\Phi(\vec{k}_k) = \tan^{-1}(\vec{v}_2 \cdot \vec{k}_k / \vec{v}_1 \cdot \vec{k}_k)$, and \vec{k}_k is defined as the *inplane* component given by

$$\vec{k}_{\kappa} = k_{\kappa} (\cos \phi_{\hat{i}} + \sin \phi_{\hat{j}}). \tag{13}$$

Since Eq. (11) is the equation of the conic section of an ellipse. Therefore, the semi-major, ℓ_{ma} , and the semi-minor, ℓ_{mi} , axislengths are respectively given as follows:

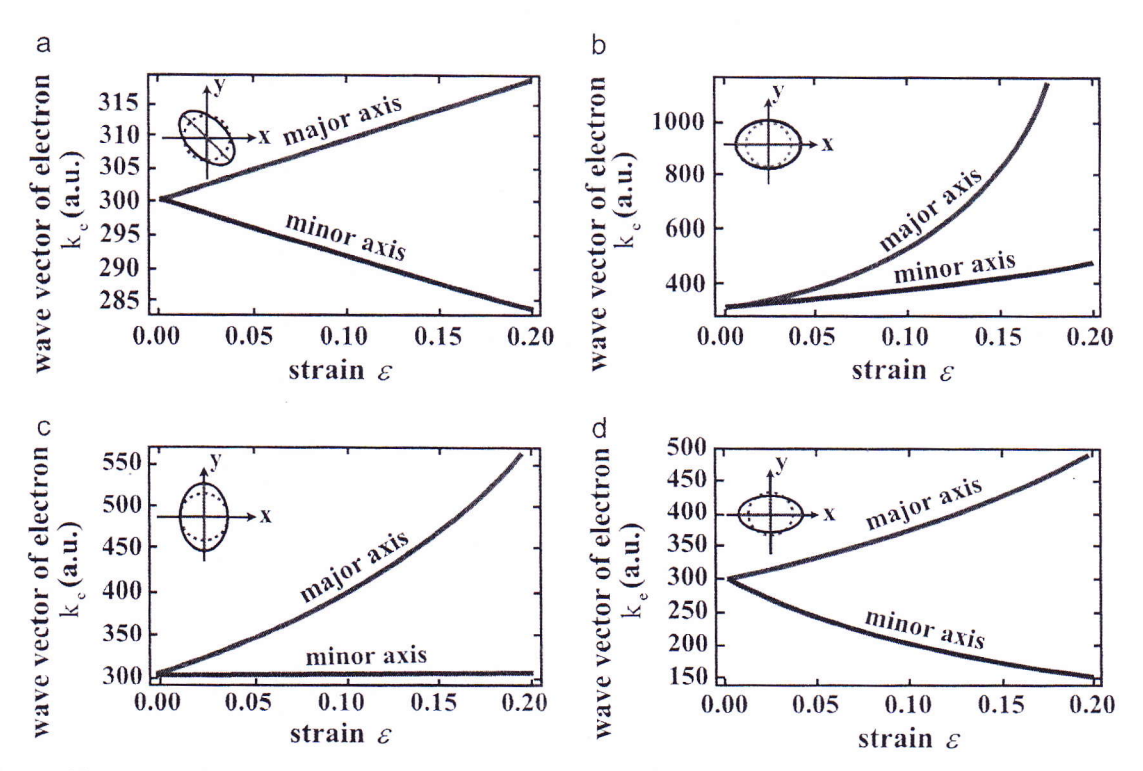


Fig. 2. The lengths of the major-axis (blue line) and minor-axis (red line) of the elliptical Fermi surface as a function of strain parameter $\epsilon \in [0.0.2]$ when (a) shear strain, (b) tensile isotropic strain, (c) uniaxial armchair strain, and (d) zigzag strain are applied on the graphene sheet. The inset in each frame is the schematic of the elliptical shape transformed from the isotropic circular shape induced by the applied strains. (For interpretation of the references to color in this figure caption, the reader is referred to the web version of this paper.)

$$\ell_{ma} = \left\{ \left(\frac{\hbar}{|E_x(\vec{k})|} \right) (2(v_1^y v_1^x + v_2^y v_2^x) \cos \phi_t \sin \phi_t + (v_1^x)^2, \\
+ (v_2^x)^2) \cos^2 \phi_t + ((v_1^y)^2 + (v_2^y)^2) \sin^2 \phi_t) \right\}^{-1/2}$$
(14)

and

$$\hat{r}_{mi} = \left\{ \left(\frac{\hbar}{|E_{\kappa}(\vec{k})|} \right) \left(-2(v_{1}^{y}v_{1}^{x} + v_{2}^{y}v_{2}^{x}) \cos \phi_{1} \sin \phi_{1} + (v_{1}^{x})^{2} + (v_{2}^{x})^{2} \right), \\
\cos^{2} \phi_{1} + ((v_{1}^{y})^{2} + (v_{2}^{y})^{2}) \sin^{2} \phi_{1} \right) \right\}^{-1/2} \tag{15}$$

where ϕ_r is the angle between the major-axis and $k_{\rm x}$ -axis given by

$$\theta_{r} = \frac{1}{2} \arctan \left(\frac{2(v_{1}^{y}v_{1}^{x} + v_{2}^{y}v_{2}^{x})}{((v_{1}^{x})^{2} + (v_{2}^{y})^{2}) - ((v_{1}^{y})^{2} + (v_{2}^{y})^{2})} \right). \tag{16}$$

Eqs. (14) and (15) describe the changes in the semi-major and the semi-minor axis lengths (Fig. 2) due to the distorted lattices, tensile isotropic strain (ϵ_{is}), shear strain (ϵ_{ss}), and uniaxial arm-chair strain (ϵ_{as}), and zigzag strain (ϵ_{zs}), respectively:

$$\epsilon_{is} = \begin{pmatrix} \varepsilon & 0 \\ 0 & \varepsilon \end{pmatrix}, \quad \epsilon_{ss} = \begin{pmatrix} 0 & \varepsilon \\ \varepsilon & 0 \end{pmatrix}, \quad \epsilon_{as} = \begin{pmatrix} \varepsilon & 0 \\ 0 & -\nu\varepsilon \end{pmatrix}, \quad \epsilon_{zs} = \begin{pmatrix} -\nu\varepsilon & 0 \\ 0 & \varepsilon \end{pmatrix}$$
(17)

where ν is Poisson's ratio and ε is a strength of the strain.

We now take a closer look at the changes of semi-major, ℓ_{ma} , and the semi-minor, ℓ_{mi} , axis lengths as a function of the strain parameter, ε , for each strain tensors. As shown in Fig. 2, the graphene sheet is differently deformed under shear strain, tensile isotropic strain, uniaxial armchair strain, and zigzag strain. We

found that the Fermi line deforms from the isotropic circle into an ellipse. The reasons for such deformation can be given as follows. In the seemingly elementary cases of shear strain, uniaxial armchair strain, and zigzag strain, the ellipse results from the change in opposite direction of reciprocal lattice parameters against the real lattice parameters. Since these strains always cause the stretch in one direction and the contraction in another perpendicular direction. Thus, the circular Fermi's line is deformed into the ellipse. On the contrary, the tensile isotropic strain stretches the graphene sheet in both *x* and *y* directions. Nevertheless the nearest-neighbor vectors do not extend in the same rate due to the nature of honey-come lattices. This brings on anisotropic shrinkage of the Brillouin zone and, also, results in the elliptical Fermi's line near the Dirac points.

3. Electron-hole recombination rate in graphene under uniaxial strains

To determine the angular dependence of the intensity of the Schwingers pair state, we consider the electron–photon coupling in terms of Feynman diagrams of quantum electro–dynamics [10–12]. We incorporate the electromagnetic field through the minimal coupling $\vec{p} \rightarrow \vec{p} - e\vec{A}/c$, treating the new vector potential term as a quantized perturbation \mathbf{H}_{int} in the full Hamiltonian:

$$\mathbf{H} = \sum_{\mu=1,2} \int d^{3}\vec{r} \ \hat{\psi}^{\dagger}(\vec{r}) \left[\vec{v}_{\mu} \cdot \left(-i\hbar \vec{\nabla} - \frac{e}{c} \mathbf{A}(\vec{r}) \right) \sigma^{\mu} \right] \hat{\psi}(\vec{r}) = \mathbf{H}_{0} + \mathbf{H}_{int}$$
(18)

where $\widehat{\psi}(\overrightarrow{r})$ is the two-component spinor written in terms of the destruction (creation) operator \widehat{C}_k (\widehat{C}_k^{\dagger}), the energy eigenstate $|\chi(k_c)\rangle$, and $\varphi(z)$, which is the confinement wave function of an electron in the graphene:

$$\hat{\boldsymbol{\psi}}(\vec{r}) = \sum_{\vec{k}} \frac{1}{\sqrt{A}} (\hat{G}_{k_c} | \chi_c(\vec{k}_c)) e^{i\vec{k}_c \cdot \vec{r} - i\alpha_c t} + \hat{G}_{k_r} | \chi_v(\vec{k}) \rangle$$

$$e^{i\vec{k}_r \cdot \vec{r} - i\alpha_r t} \rho(z), \tag{19}$$

where the subscripts c and ν respectively stand for conduction and valence bands. The vector potential $\overrightarrow{A}(\overrightarrow{r})$ is given by the mode expansion such that

$$\overrightarrow{A}(\overrightarrow{r}) = \sum_{k_r,j} c \sqrt{\frac{2\pi\hbar}{\varepsilon_r \omega_k V}} (\widehat{a}_{k_r,j} \widehat{\varepsilon}_j e^{i\overrightarrow{k_r} \cdot \overrightarrow{r} - i\alpha_r t} + \widehat{a}_{k_r,j}^{\dagger} \widehat{\varepsilon}_j e^{-i\overrightarrow{k_r} \cdot \overrightarrow{r} + i\alpha_r t})$$
(20)

where $\hat{a}_{k_{r}j}$ ($\hat{a}_{k_{r}j}^{\dagger}$) is the photon annihilation (creation) operator and j indexes the photons polarization state, ϵ_{r} is the relative permittivity, V is the normalization volume, and $a_{ij} = c_{ij} \vec{k_{r}}$. We define the direction of radiation $\hat{k_{r}}$ and the polarization unit vectors, $\hat{\epsilon}_{1(2)}$, as follows:

$$\hat{k}_{\gamma} = (\sin \theta_{\gamma} \cos \phi_{\beta}, \sin \theta_{\gamma} \sin \phi_{\gamma}, \cos \theta_{\gamma}), \tag{21}$$

$$\hat{\varepsilon}_1 = \left(-\sin \, \phi, \cos \, \phi\right). \tag{22}$$

and

$$\hat{\varepsilon}_2 = \left(-\cos \theta_r \cos \phi_r, -\cos \theta_r \sin \phi_r, \sin \theta_r\right), \tag{23}$$

where ϕ is the azimuthal angle, and ϕ is the polar angle.

The transition rate $I_{i \to f}$ which is the rate of the transition from the initial electronic state $|\psi_f\rangle$ into the final electronic state $|\psi_f\rangle$ owing to the electron–photon interaction. It can be obtained from the standard arguments of Fermi Golden Rule:

$$F_{i-f} = \frac{d}{dt} |\langle \psi_f(t) | \Psi(t) \rangle|^2, \tag{24}$$

where

$$\langle \psi_f(t) | \Psi(t) \rangle \approx \frac{1}{i\hbar} \int_0^t dt' \langle \psi_f(t') | \mathbf{H}_{int}(t') | \psi_f(t') \rangle. \tag{25}$$

Our calculation is based on the simplest tree-level Feynman diagram. The vertex connects a photon with two electrons by means of Fermi golden rule. However, the second order term, corresponding to two-photon emission process, has an order of

magnitude $(v_F/c)^2$. The very small of v_F/c , $\sim 1/300$, is responsible for neglecting this term and higher order terms in the calculation of R_{-f} . In the simplest approach, the electron transport is purely ballistic process, thus neglecting impurities. It is able to get good agreement for near zero temperature [20]. For a deeper analysis, behavior of the conductivity and the number of electron-hole pairs in the various regimes at finite electric field E was discussed in ref. [21]. We, next, consider a process that creates a valence electron $|\psi_f(t)\rangle \propto |\chi_c(\hbar \vec{k}_c)\rangle$ ((in the valence band) and a photon $|\hbar \vec{k}_r\rangle$ with polarization \hat{e}_j whereby destroying a conduction electron $|\psi_f(t)\rangle \propto |\chi_c(\hbar \vec{k}_c)\rangle$ (in the conduction band). To calculate the differential rate $dI_{C\rightarrow V}$ of the process defined by Eq. (24), we insert Eq. (25) into Eq. (24) and then multiply by $d^2\vec{k}_V$ $d^3\vec{k}_c$:

$$\begin{split} dI_{c\rightarrow v}^{*} &= \left(\frac{e^{2}v_{F}^{2}}{2\pi\epsilon_{F}\omega_{k}}\right) \mathcal{M}(\theta_{F}, \phi_{F}, \epsilon) n_{c} (\overrightarrow{k_{c}}) (1 - n_{v} (\overrightarrow{k_{v}})) (1 + n_{v} (\overrightarrow{k_{v}})) \\ &\times \left[\delta(\hbar\omega_{v} + \hbar\omega_{F} - \hbar\omega_{c})\delta^{2} (\overrightarrow{k_{v}} + \overrightarrow{k_{v}} - \overrightarrow{k_{c}})\right] d^{2}\overrightarrow{k_{v}} d^{3}\overrightarrow{k_{r}}. \end{split} \tag{26}$$

The distribution of the energy eigenstates of the electrons in conduction and valence bands are given by the Fermi-Dirac distribution functions. $n_{\kappa}(\vec{k_{\kappa}})$ and $n_{\gamma}(\vec{k_{\gamma}})$ are the Bose-Einstein distribution functions. The photon emission distribution radiated from the surface of the sample is characterized by the angular matrix element, i.e.

$$\mathcal{M}(\theta_r, \phi_r, \varepsilon) = \frac{1}{v_F^2} \sum_{\mu, j} \left| \langle \chi_r(\vec{k}_v) | \vec{V}_{\mu} \sigma^{\mu} \cdot \hat{\mathcal{E}}_j | \chi_c(\vec{k}_c) \rangle \right|^2, \tag{27}$$

and $n_c(\vec{k}_c)$ and $1 - n_v(\vec{k}_v)$ respectively are the number of conduction electrons and the number of holes. It is obvious, from Eq. (26), that the recombination rate is proportional to the number of conduction electrons $n_c(\vec{k}_c)$ and the number of holes $1 - n_v(\vec{k}_v)$.

In evaluating Eq. (26), we must keep in mind the energy conservation and the momentum conservation requirements. Those are

$$E_{v}(\overrightarrow{k}_{v}) = E_{c}(\overrightarrow{k}_{c}) - \hbar c \overrightarrow{k}_{y} I, \qquad (28)$$

and

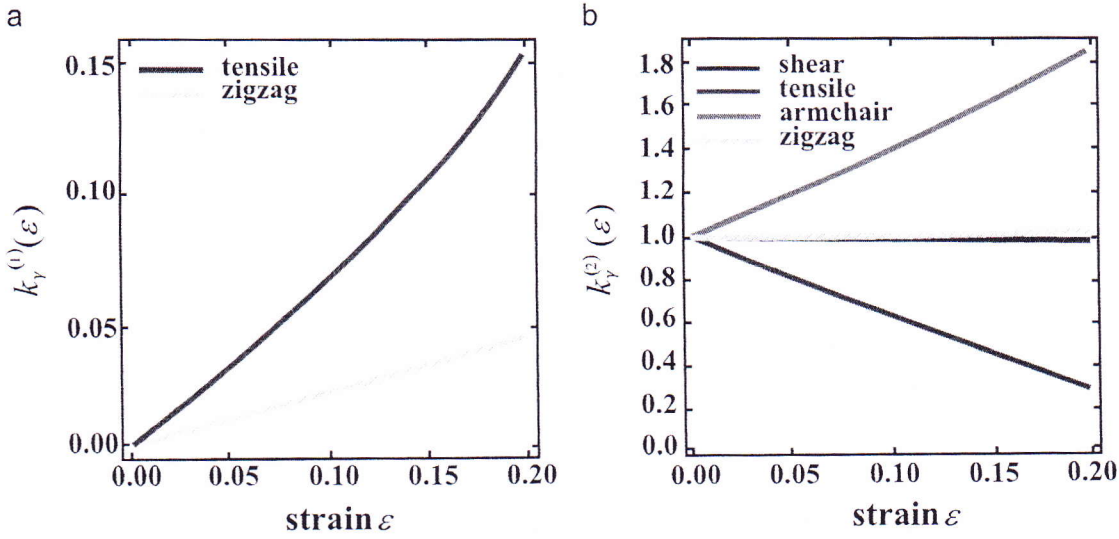


Fig. 3. Strain dependencies of (a) $k_y^{(1)}$, and (b) $k_y^{(2)}$ calculated from Eq. (33) with $\varepsilon \in [0, 0.2]$.

$$\vec{k}_{v} = \vec{k}_{c} - \vec{k}_{y}^{\parallel}, \tag{29}$$

where $\vec{k}_{\gamma}^{\parallel}$ is the photon momentum parallel the graphene plane. Note that in the integration procedure of Eq. (26) we use the relation

$$\delta(f(x)) = \sum_{i} \frac{1}{\left|\frac{\partial f(x_{i})}{\partial x_{i}}\right|} \delta(x - x_{i}); f(x_{i}) = 0.$$

$$(30)$$

We can define the strain dependent photon emission rate, which is propositional to the radiation intensity, as

$$\begin{split} \frac{dI_{c \to v}(\varepsilon)}{d\Omega_{\gamma}} &= \alpha \left(\frac{v_F^2}{\pi \varepsilon_r \, \omega_c} \right) \mathcal{M}(\theta_r, \, \phi_r, \, \varepsilon) \\ &\qquad \qquad \sum_{i=1,2} n_c \, (E_c) (\hat{1} - n_v \, (E_v)) (1 + n_\gamma \, (k_\gamma^{(i)})) l k_\gamma^{(i)} l^2, \end{split} \tag{31}$$

where $\alpha = e^2/\hbar c$ denotes the fine-structure constant, i.e. an unit of optical reflectivity or transmission magnitude [22]. Here $k_y^{(i)}$'s are the photon momenta satisfying the energy conservation and the momentum conservation conditions, given by

$$k_{\gamma}^{(1)} = \frac{-B + \sqrt{B^2 - 4AC}}{2A}, \quad k_{\gamma}^{(2)} = \frac{-B - \sqrt{B^2 - 4AC}}{2A}$$
 (32)

where A, B and C are defined as follows:

$$A = -c^{2} + (v_{1}^{x}v_{1}^{y} + v_{2}^{x}v_{2}^{y})\sin(2\phi_{1})\sin^{2}\theta_{2}$$

$$+ \left(((v_{1}^{x})^{2} + (v_{2}^{x})^{2})\cos^{2}\phi_{1} + ((v_{1}^{y})^{2} + (v_{2}^{y})^{2})\sin^{2}\phi_{2}\right)\sin^{2}\theta_{2}, \quad (33)$$

$$B = \frac{2cE_{c}}{\hbar} - 2k_{c} \sin \theta_{r} \left(((v_{1}^{x})^{2} + (v_{2}^{x})^{2}) \cos \phi_{r} \cos \phi_{r} + ((v_{1}^{y})^{2} + (v_{1}^{y})^{2}) \sin \phi_{r} \sin \phi_{r} - (v_{1}^{x}v_{1}^{y} + v_{2}^{x}v_{2}^{y}) \sin(\phi_{r} + \phi_{r}) \right),$$
(34)

$$C = -\frac{E_c^2}{\hbar^2} + k_c^2 (v_1^x v_1^y + v_2^x v_2^y) \sin(2\phi_t) + k_c^2 ((v_1^x)^2 + (v_2^x)^2)$$

$$\cos^2 \phi_t + k_c^2 ((v_1^y)^2 + (v_2^y)^2) \sin^2 \phi_t.$$
(35)

Photon wave vectors $k_{\gamma}^{(1)}$ and $k_{\gamma}^{(2)}$ arising from a particular strain profile obey the following limitations:

$$\lim_{\varepsilon \to 0} k_{\gamma}^{(1)} = 0, \quad \lim_{\varepsilon \to 0} k_{\gamma}^{(2)} = k_{\gamma}^{(0)}, \quad k_{\gamma}^{(i)} > 0; \quad i = 1, 2$$
(36)

where $k_{\gamma}^{(0)}$ is a photon wave vector for unstrained graphene which was calculated by Mecklenburg et al. in Ref. [10]. It has the maximum value at $\phi = \phi$.

Let us consider the analytic expressions for the effects of the lattice distortion on the photon wave vectors $k_{\gamma}^{(1)}$ and $k_{\gamma}^{(2)}$ (Eq. (32)). For numerical calculation,we assume a perfect population

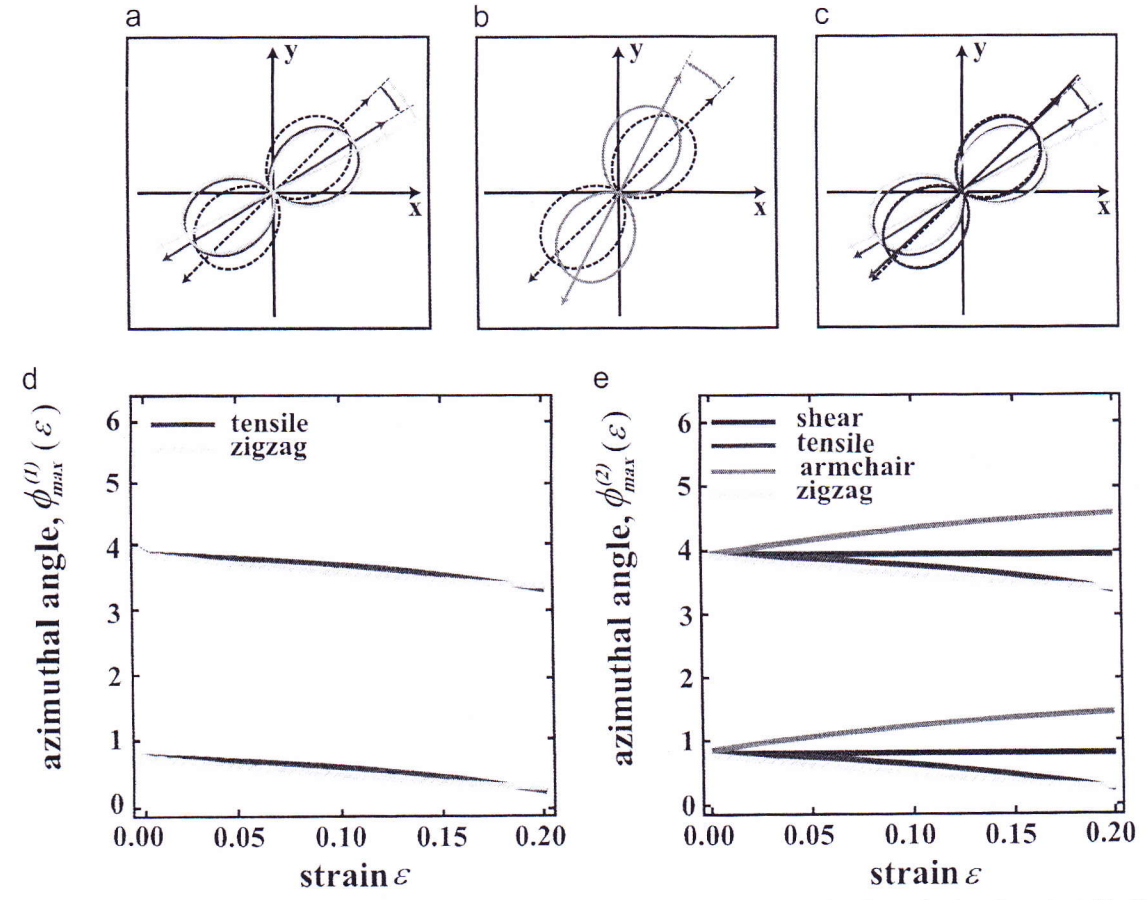


Fig. 4. (a)–(c) Rotations of the radiation directions due to the applied strains (colors) compared to the radiation direction of unstrained graphene sheets (black), $\phi_c = \pi/4$. (a) The rotations attributed to $k_f^{(1)}$ in a.u., (b) and (c) The rotations attributed to $k_f^{(2)}$. (b) is separated from (c) to distinguish its anticlockwise rotation from the clockwise ones. (d) and (e) represent the azimuthal angles of $k_f^{(1)}$ and $k_f^{(2)}$ as a function of strain parameter respectively, and sets of upper lines are $\phi_{max}^{(0)}$ whereas sets of lower ones are $\phi_{min}^{(0)}$. The colors indicate the types of strains. (For interpretation of the references to color in this figure caption, the reader is referred to the web version of this paper.)

inversion, $n_c = 1$ and $n_v = 0$, and a conduction electron energy $\hbar\omega_{\rm c}=1~{\rm eV}$. We first look at the effects of the strain tensors and their strengths on the magnitude of photon wave vector $k_s^{(j)}$ (per unit $k_0 = \omega_c/c$). From the numerical evaluations with the strain parameter $\varepsilon \in [0, 0.2]$, we found that in case of uniaxial armchair strain $k_{\gamma}^{(1)}$ can be either positive number or negative number, but the latter is not allowed, while it is only positive number otherwise. In addition, $k_x^{(1)} \rightarrow 0^+$ for both armchair strain and shear strain as the cases. These are the reasons why these cases are not shown in Fig. 3(a). The strain dependencies of $k_r^{(1)}$ and $k_r^{(2)}$ are shown in Fig. 3. For tensile isotopic strain, $k_r^{(1)}$ increases from 0 to 0.15 (a.u.) and $k_v^{(2)}$ decreases from 1 to 0.2 (a.u.). The photon emission intensity appears to be reduced as increasing ε . For shear strain, $k_r^{(2)}$ slightly decreases and so the photon emission intensity tends to be constant. For uniaxial zigzag strain, $k_x^{(1)}$ increases from 0 to 0.05 (a.u.) whereas $k_x^{(2)}$ is constant at 1. The photon emission intensity tends to increase, slightly, as increasing ε . For uniaxial armchair strain, $k_x^{(2)}$ increases from 1 to 1.8 (a.u.) which roughly is twice its initial value. Thus, the photon emission intensity increases as increasing ε .

Second, we determine the directions that are attributed to the radiation modes $\vec{k}_{\gamma}^{(i)}$'s. There are two contributions from $\vec{k}_{\gamma}^{(1)}$ and $\vec{k}_{\gamma}^{(2)}$ modes to the intensity. We denote the intensities contributed from $\vec{k}_{\gamma}^{(i)}$ as $I^{(i)}$. Since $I^{(i)}$ is propositional to $|\vec{k}_{\gamma}^{(i)}|^2$ the direction at

which $I^{(i)}$ reaches its maximum can be determined by the condition $(dk_{\gamma}^{(i)}/d\phi)|_{\phi=\phi_{max}^{(i)}}=0$. We found, from the numerical evaluation, that $\phi_{min}^{(i)}=\phi_{max}^{(i)}\pm\frac{\pi}{2}$. Furthermore, there are the rotations of the radiation directions caused by the applied strains. The rotations of $k_{\gamma}^{(1)}$ and $k_{\gamma}^{(2)}$ radiation modes are both clockwise rotations with respect to ϕ_c due to tensile isotropic strain and uniaxial zigzag strain. Also, the radiation direction of $k_{\gamma}^{(2)}$ mode is clockwise rotation when shear strain is applied to the graphene sheet. Surprisingly, when the armchair strain is applied the rotation of $k_{\gamma}^{(2)}$ mode is counterclockwise rotation, see Fig. 4(a)–(c). The influence of strains to the radiation directions is shown in Fig. 4(d) and (e). Moreover, since $|k_{\gamma}^{(1)}|^2 \ll |k_{\gamma}^{(2)}|^2$ the direction of total radiation can approximately be identified by $\phi_{max}^{(2)}$. That is $\phi_{max} \simeq \phi_{max}^{(2)}$

Finally, we consider the relative photon emission rate in the xy plane compared to the unstrained distribution of the Schwinger pair creation. For the unstrained case, $\varepsilon=0$, the photon emission depends on the azimuthal angle ϕ measured from the armchair direction of graphene sheet similar to the radiation from accelerated charged particles, as discussed in ref. [10]. The relative photon emission rate, which is propositional to the relative radiation intensity, is given by

$$\frac{d\Gamma(\phi, \varepsilon)}{d\Omega_{\gamma}} = \frac{dI_{c \to v}(\phi, \varepsilon)}{d\Omega_{\gamma}} - \frac{dI_{c \to v}(\phi, 0)}{d\Omega_{\gamma}}.$$
(37)

Fig. 5 shows the relative intensity, obtained from Eq. (37), as a

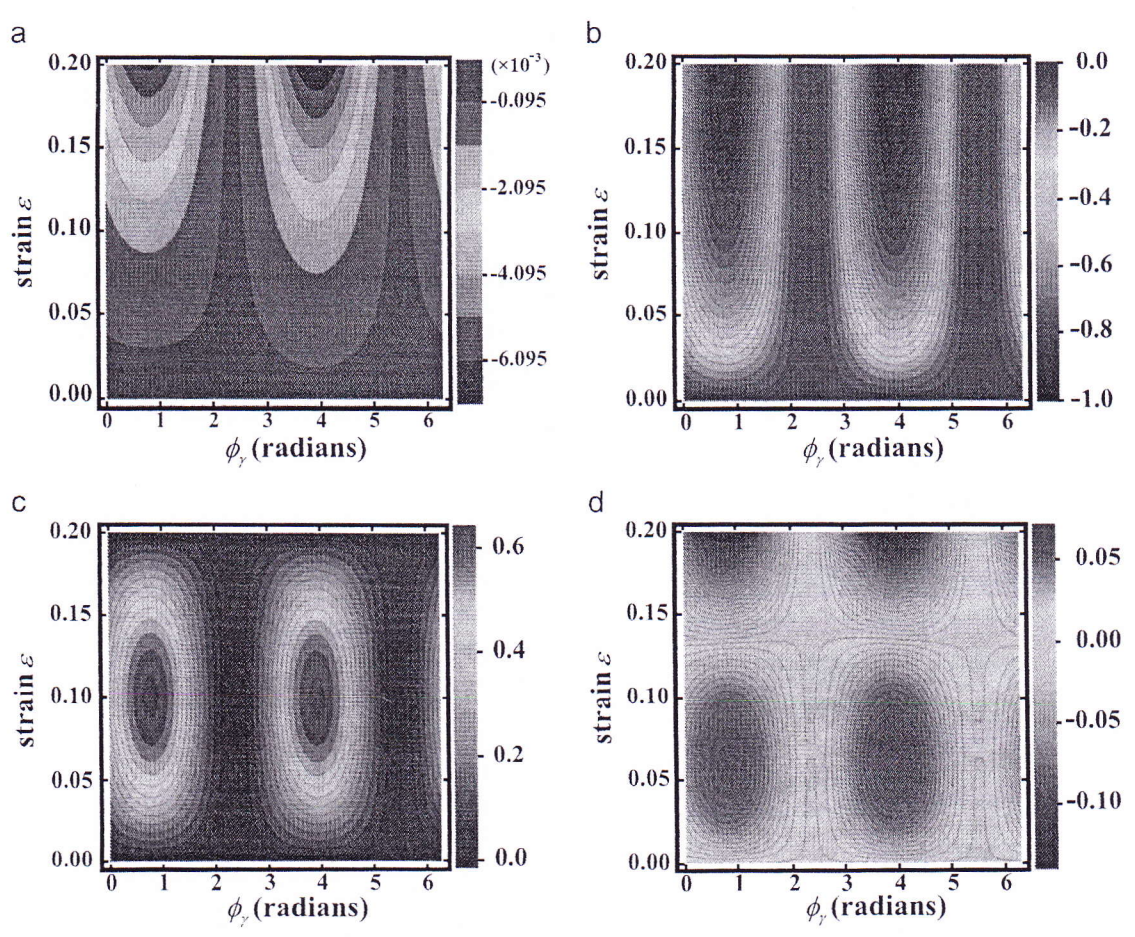


Fig. 5. Contour plot of relative radiation intensity under (a) shear strain, (b) tensile isotropic strain, (c) uniaxial armchair strain, and (d) zigzag strain, with varied strength of the strain ε and an angle ϕ , the angle measured counterclockwise from the k_r^x -axis. With initial $n_c = 1$ and $n_r = 0$ in calculating Eq.(32), this process corresponds to the emission from an initial electron moving along \vec{k}_c with $\phi_c = \pi/4$.

function of the strength of the strain ε and ϕ . It clearly shows that the applied shear strain and tensile isotropic strain soften the radiation intensity, Fig. 5(a) and (b). In contrast, the uniaxial armchair strain strengthens the radiation intensity, Fig. 5(c). Sensationally, the zigzag strain can alternatively induce both intensity softening and strengthening. This depends on the strength of applied strain. The intensity strengthening is in the strain range $\varepsilon^{(+)} \in (0, 0.13)$ while the intensity softening is in the range $\varepsilon^{(-)} \in (0.13, 2)$, approximately. To simply illustrate the time scales $\tau = \Gamma(\varepsilon)^{-1}$ for decay spontaneously emission in electron-hole recombination, we numerically integrate Eq. (37) over all directions of \vec{k}_{x} . Since $\sum |k_{x}^{(i)}|^{2}$ is fairly uniform function of ϕ the superb result can be easily carried out by fixing $k_{\gamma}^{(i)} = k_{\gamma}^{(i)}(\phi_{max})$. We approximately obtain

$$\Gamma(\varepsilon) \simeq \alpha \eta(\varepsilon); \quad \eta(\varepsilon) = \Gamma_0 \mathcal{M}(\varepsilon) \sum_{i=1}^{2} \left(|k_y^{(i)}(\phi_y^{(max)}, \varepsilon)|^2 - 1 \right)$$
 (38)

where $\Gamma_0 = 8v_F^2 k_0^2/3\epsilon_F \omega_c$, and $\mathcal{M}(\epsilon)$ is the characteristic function of the angular matrix element for each type of strains given by

$$\mathcal{M}(\varepsilon) = a\varepsilon^3 + b\varepsilon^2 + c\varepsilon + d. \tag{39}$$

The coefficients a, b, c, and d, for each strain, are given as follows: a = 0, b = -20.52, c = 2.45, and d = 1 for zigzag strain; a = 174.93, b = -68.46, c = 2.96, and d = 1 for uniaxial armchair strain; a = 0, b = 0, c = -4.768, and d = 1 for tensile isotropic strain; and a = 0, b = 0, c = 0.59, and d = 1 for shear strain. These set forth that $\mathcal{M}(\varepsilon)$ is a polynomial function of ε with different degrees for each applied strains. It is quadratic function for zigzag strain, cubic function for armchair strain, and linear function for tensile and shear strains.

4. Conclusions

In this work, we have investigated the electron dynamics of electrons hopping on the honeycomb lattice of graphene which had been deformed. The underlying dynamics is governed by a nearest-neighbor tight-binding Hamiltonian, which for graphene is the Weyl-Dirac equations. Deformation of the lattice leads to modified hopping energy and to shifts in the lattice points. These modifications are treated as a slowly varying perturbation to the Hamiltonian. We find that the corrections to two velocities can be described in terms of four parameters which depend on the strain tensor ϵ . For strains of the order of 20% the Fermi line is deformed from the isotropic circular shape to an elliptic shape. It is also shown that the structure of energy band, the frequency of the photon and emission distribution can be controlled by the mechanical strains.

Acknowledgments

We are grateful to Prof. I-Ming Tong and C. Sricleewin for useful discussions. We acknowledge the financial support by Department of Physics, Faculty of Science, Kasetsart University, for partial support. A. H. wishes to thank Physics Division, Faculty of Science and Technology, Phetchabun Rajabhat University, Thailand.

References

- K.S. Novoselov, et al., Science 306 (2004) 656.
- K.S. Novoselov et al., Proc. Natl. Acad. Sci USA, 102 (2005) 10451.
- [3] C.W.J. Beenakker, Rev. Mod. Phys. 80 (2008) 1337.
 [4] V.V. Cheianov, et al., Science 315 (2007) 1252.
 [5] A.L. Kitt, et al., Phys. Rev. B 85 (2012) 115432.

- [6] F. Bonaccorso, et al., Nat. Photon. 4 (2010) 611
- [7] A.H.Castro, Neto, et al., Rev. Mod. Phys. 81 (2009) 109.[8] K.F. Mak, et al., Phys. Rev. Lett. 101 (2008) 196405.
- S.M. Choi, et al., Phys. Rev. B 81 (2010) 081407.
- [10] M. Mecklenburg, et al., Phys. Rev. B 81 (2010) 245401.[11] M. Lewkowicz, et al., Phys. Rev. B 84 (2011) 035414.
- [12] B. Rosenstein, et al., J. Phys.: Conf. Ser. 400 (2012) 042051.
- [13] J. Schwinger, Phys. Rev. 82 (1951) 664.
- V.M. Pereira, et al., Phys. Rev. B 80 (2009) 045401.
- [15] A.H. Castro Neto, et al., Rev. Mod. Phys. 81 (2009) 109-162. Y. Hasegawa, et al., Phys. Rev. B 74 (2006) 033413.
- A.L. Kitt, et al., Phys. Rev. B 85 (2012) 115432.
- [18] F. de Juan, et al., Phys. Rev. B 76 (2007) 165409.
 [19] R.O. Dillon, et al., J. Phys. Chem. Solids 38 (1977) 635.
- [20] K.I. Bolotin, et al., Phys. Rev. Lett. 101 (2008) 096802.
- [21] H.C. Kao, et al., Phys. Rev. B 82 (2010) 035406.
- [22] K.F. Mak, et al., Phys. Rev. Lett. 101 (2008) 196405.